https://doi.org/10.5194/egusphere-2025-2555
Preprint. Discussion started: 15 July 2025


# How meteorological conditions influence aerosol-cloud interactions under different pollution regimes

Jianqi Zhao[1,2], Xiaoyan Ma[1], Johannes Quaas[2] and Tong Yang[1]

[1]China Meteorological Administration Aerosol-Cloud and Precipitation Key Laboratory, Nanjing University of Information Science and Technology, Nanjing 210044, China

[2]Leipzig Institute for Meteorology, Leipzig University, Leipzig, Germany

Correspondence: Xiaoyan Ma (xma@nuist.edu.cn)

**Abstract.** Aerosol-cloud interactions (ACI) involve quite complex physical and dynamical mechanisms, in which meteorological conditions play a crucial role. To investigate how the meteorological conditions impact ACI under different pollution regimes (polluted and clean) for marine liquid-phase clouds, the simulations are conducted using the chemistry version of Weather Research and Forecasting Model coupled with spectral-bin cloud microphysics. Our results indicate that, marine liquid-phase clouds transition from being updraft-driven to cold-advection-driven as lower tropospheric stability (LTS) increases. The enhancement of these clouds by aerosols intensifies with LTS, highlighting the dominant role of cold advection on wintertime clouds. Aerosols prolong cloud lifetime in moist environments and shorten it in dry environments. They generally suppress precipitation but can enhance it during some intense cloud processes by promoting cloud vertical development and collision-coalescence. The influences of meteorological conditions on ACI exhibit distinct differences between the two pollution regimes. Under the clean regime, activation efficiency shows low sensitivity to meteorological conditions, enabling aerosols in clouds to fully activate across most environments, while the aerosol-limited state and the dominance of condensation lead to increases in cloud droplet size, cloud liquid water path, and rainwater path with supersaturation. In contrast, under the polluted regime, ACI are more sensitive to relative humidity than under the clean regime, and clouds respond oppositely to aerosols under different LTS conditions. Additionally, the dominance of collision-coalescence leads to initial cloud intensification followed by weakening with supersaturation.

## 1 Introduction

Aerosol-cloud interactions (ACI) remain one of the major sources of uncertainty in climate assessment and prediction (IPCC, 2023). The complexity of aerosol impacts on clouds under varying meteorological conditions (Ma et al., 2018; Jia et al., 2019a; Anwar et al., 2022), along with difficulties in assessing these effects, constitutes a dominant contributor to uncertainty in ACI (Lohmann and Feichter, 2005; McComiskey and Feingold, 2012).

Liquid-phase clouds are the main contributors to the total impact of aerosols on clouds due to their broad coverage, high optical thickness, and often long lifetime (Chen et al., 2011; Andersen et al., 2017; Jia et al., 2019b). In addition, this type of cloud is highly sensitive to aerosol (Chen et al., 2014; Jia et al., 2019b). In liquid-phase clouds, ACI are primarily based on two mechanisms: (1) the Twomey effect, i.e. the entry of additional aerosol into the cloud leads to an increase in the cloud droplet number concentration ($N_d$), a decrease in the cloud droplet effective radius (CER), and an increase in cloud albedo under constant cloud water content (Twomey, 1977). (2) Rapid adjustments, consist of the response of cloud liquid water path (CLWP) and cloud fraction to changes in $N_d$ via the Twomey effect (Albrecht, 1989; Haghighatnasab et al., 2022; Jia et al., 2022).

The effects of these mechanisms are modulated by meteorological conditions. Observation-based studies using ground-based measurements indicate that as boundary layer moisture increases, the impact of aerosols on cloud microphysics becomes more pronounced (Zheng et al., 2022). Analyses of satellite and reanalysis data reveal a positive

https://doi.org/10.5194/egusphere-2025-2555
Preprint. Discussion started: 15 July 2025


correlation between CER and both lower tropospheric stability (LTS) and relative humidity (RH) over the East China Sea (Liu et al., 2024). Updraft is one of the primary drivers of aerosol–cloud interactions (Salma et al., 2021), but its influence varies in different environments. For instance, Liu et al. (2024) identified a negative correlation between CER and pressure vertical velocity over the East China Sea. Reutter et al. (2009) and Hudson and Noble (2014) demonstrated, based on simulations and observations respectively, the sensitivity of ACI to updraft under varying aerosol number concentrations ($N_a$). Furthermore, large-scale circulation also plays a significant regulatory role in ACI (Dagan et al., 2023). Under the combined influence of these meteorological factors, ACI form a complex nonlinear system. Observational analysis of this system suffers severely from retrieval uncertainties (Arola et al., 2022) and interference from the radiative effects of aerosols and clouds (Sakaeda et al., 2011; Zelinka et al., 2014), thus requiring integration with numerical simulations. This study employs the WRF-Chem-SBM model (Gao et al., 2016), which couples the online-chemistry version of the Weather Research and Forecasting model (WRF-Chem) with the spectral bin cloud microphysics (SBM) scheme, to analyze the sensitivity of ACI to meteorological conditions in different environments. As an online coupled model integrating SBM and a sectional aerosol module, it demands higher computational resources but significantly improves aerosol-cloud simulation capabilities compared to commonly used bulk cloud microphysics (Khain et al., 2015; Zhang et al., 2021).

In our previous study (Zhao et al., 2024), by reproducing and analyzing a factual scenario during winter (characterized by the highest frequency of low clouds (Chang et al., 2021; Niu et al., 2022)) over Eastern China (EC, one of the major anthropogenic aerosol source regions worldwide) and its adjacent ocean (ECO), we evaluated the simulation capability of the WRF-Chem-SBM model, and obtained insights into the general patterns, primary physical mechanisms, and influencing factors of ACI in liquid-phase clouds. Building on previous study, we investigate how the effects of continental aerosols on liquid-phase clouds and ACI under different pollution regimes respond to meteorological conditions over ECO in this study. By focusing on marine liquid clouds and disabling the radiative effects of aerosols and clouds, this study largely eliminates interference from terrain (Zhao et al., 2024) and radiative effects, enabling explicit analysis of ACI.

## 2 Methods and data

### 2.1 WRF-Chem-SBM model

This study utilizes the WRF-Chem-SBM model (Gao et al., 2016), which couples the Model for Simulating Aerosol Interactions and Chemistry (MOSAIC) aerosol module (four-bin) of the WRF-Chem model and the SBM scheme, to perform aerosol-cloud simulation. The MOSAIC aerosol module treats the mass and number distributions of the nine main aerosol species (sulfate, nitrate, chloride, ammonium, sodium, black carbon, primary organics, other inorganics, and water). The aerosol particles are assumed to be internally mixed (Zaveri et al., 2008). The diameters of the four bins range from 0.039-0.156, 0.156-0.624, 0.624-2.5 and 2.5-10.0 μm, respectively. The module treats processes such as aerosol emissions, gas-particle transition, coagulation, in-cloud liquid-phase chemistry, dry deposition, and wet scavenging (Sha et al., 2019; Sha et al., 2022). The SBM scheme in this model is the fast version, which solves a system of prognostic equations for three hydrometeor types (droplets, ice/snow, and graupel) and CCN, by numerically discretizing their size distributions. Each size distribution function is structured into 33 mass-doubling bins, wherein the mass within the k-th size bin is twice that within the (k-1)-th bin. This scheme can treat cloud microphysics processes such as aerosol activation, freezing, melting, diffusion growth/evaporation of droplets, deposition/sublimation of ice particles, droplets, and ice collisions (Khain et al., 2004).

In this coupled model, aerosols from MOSAIC are distributed into 33 CCN bins based on their physical and chemical properties and are then processed through the aerosol activation, resuspension, and in-cloud wet removal parameterizations in SBM, which not only impact cloud microphysics but also provide feedback to the aerosol module. The aerosol activation parameterization in this model is based on the Köhler theory, which calculates the critical supersaturations ($S_{crit}$) at the

https://doi.org/10.5194/egusphere-2025-2555
Preprint. Discussion started: 15 July 2025


boundary sizes for each CCN bin. When the prognostic supersaturation falls between the boundary-size $S_{crit}$ of a given bin, the CCN in that bin are fractionally activated. CCN in larger bins with lower $S_{crit}$ are completely activated, while CCN in smaller bins do not undergo activation (Gao et al., 2016).

## 2.2 Observational data

In order to evaluate the simulated meteorological conditions, aerosols, clouds, and precipitation, various observational datasets are utilized, including height, temperature, dew point depression, and wind field (at 11 pressure layers, 12 hours temporal and 2.5° spatial resolutions) from the Meteorological Information Comprehensive Analysis and Processing System (MICAPS, Hu et al., 2018) developed by the National Meteorological Center of China, hourly near-surface $PM_{2.5}$ data from more than 1600 stations provided by the National Urban Air Quality Real-time Release Platform (China National Environmental Monitoring Center, 2023), AOD from the MOD04_L2 dataset (Levy et al., 2015) which combines the "Dark Target" and "Deep Blue" algorithms with temporal and spatial resolutions of 5 min and 10 km, as well as cloud parameters (such as CER, cloud optical thickness (COT), and CLWP) from the MOD06_L2 dataset (Platnick et al., 2015) with temporal and spatial resolutions of 5 min and 1 km. The column-integral $N_d$ is calculated from COT and CER based on the approach of Han et al. (1998, see also Brenguier et al. (2000)):

$$N_d = \gamma \cdot COT^{0.5} \cdot CER^{-2.5} \quad (1)$$

where γ is a constant valued at $1.37 \times 10^{-5}$ $m^{-5}$ (Quaas et al., 2006). In addition, the 5-min temporal resolution of MOD04_L2 and MOD06_L2 data originates from the satellite's scanning frequency. However, since the Terra satellite passes over a fixed location only once per day, the actual temporal resolution of these data for a specific region is 1 day.

Precipitation data is obtained from the Integrated Multi-satellitE Retrievals for GPM (IMERG) dataset (Huffman et al., 2019), of which the daily accumulated high quality precipitation product is used in this study, with a temporal and spatial resolution of 1 day and 0.1°, respectively.

## 2.3 Data processing

Due to the resolution differences between the observations and simulations, interpolation is needed before comparing them. Specifically, for observational data with higher resolution than the model grid, the observational data is interpolated to the model grid, while for observational data with lower resolution than the model grid, the simulation data is interpolated to the grid of the observational data.

When comparing the spatial distribution of simulation results with satellite-retrieved data averaged over the study period, it is unreasonable to directly compute the average of the simulation results for the entire period due to the spatio-temporal discontinuities of satellite-retrieved data. Therefore, to make the comparison with the satellite-retrieved data, spatio-temporal matching is performed for the simulation data. Specifically, only when satellite data at a given grid point and time is valid, the corresponding simulation value is included in the average calculation.

In addition to the above, further processing is required for both satellite-retrieved and simulated liquid-phase cloud parameters. For MODIS cloud parameters, cloud retrievals with high reliability are selected using the method referenced from Saponaro et al. (2017): (1) Liquid-phase cloud data are chosen based on MODIS cloud phase parameters, and (2) transparent-cloudy pixels (COT < 5) are screened out to limit uncertainty (performing this screening results in the inability to evaluate simulations with low COT pixels, reducing the completeness of the evaluation but increasing its reliability). When calculating the simulated cloud parameters for a specific grid point, in cases where multiple independent clouds exist at different altitudes, we follow the method of the instrument simulator, treating these clouds as if they are from a single homogeneous layer (Pincus et al., 2012). When comparing the simulations with satellite-retrieved cloud parameters, we refer to the processing of satellite-retrieved cloud parameters and the threshold method used by Roh et al. (2020) for distinguishing cloud phases. The following criteria are applied to filter the simulated cloud parameters: (1) cloud optical

https://doi.org/10.5194/egusphere-2025-2555
Preprint. Discussion started: 15 July 2025


thickness of water (COTW) > 0.1 and cloud optical thickness of ice (COTI) < 0.01 for each layer, and (2) column COTW ≥ 5. The simulated COTW and COTI used in this study are calculated based on the methodology in the Goddard radiation scheme (Zhong et al., 2016) of the WRF-Chem model. Additionally, in the evaluation, the method used to calculate simulated $N_d$ is the same as that used for satellite-retrieved $N_d$. In the analysis of the simulation results, $N_d$ is directly taken from the model output, and the criteria for liquid-phase clouds are strictly defined as cloud liquid water content (CLWC) > 0 and cloud ice water content (CIWC) = 0 (the processing of the simulation results at evaluation is no longer used in the analysis).

We employ multiple statistical metrics to support the analysis. Data uncertainty is quantified using the 25th-75th percentile range, mean, median, 1.5 interquartile range (IQR), and outlier. Pearson correlation is used to assess relationships between variables. For datasets with complete spatiotemporal coverage, correlations are computed at each grid point. In the case of multi-layer datasets, values are interpolated to common vertical levels and reshaped into one-dimensional arrays ordered from bottom to top. For datasets with limited spatiotemporal completeness (fewer than five time series or coverage below 60% of the model domain), we apply the uncentered Pearson product-moment coefficient to evaluate spatial correlations of grid point means. Relative differences between parameters are assessed using the Normalized Mean Bias (NMB).

## 3 Experiment design and model evaluation

### 3.1 Case description

This study aims to investigate how the effects of continental aerosols on liquid-phase clouds and ACI under different pollution regimes respond to meteorological conditions over ECO (highlighted by the red box in Fig. 1). For this purpose, we (1) design two experiments—Control (polluted regime, including both continental and marine emissions) and Clean (clean regime, including only marine emissions)—to qualitatively and quantitatively analyze the sensitivity of ACI to meteorological conditions in different environments, and (2) select a short-term case characterized by substantial variability in meteorological, aerosol, and cloud parameters (liquid-phase clouds over ECO from February 1 to 5, 2019), balancing computational cost with analysis comprehensiveness.

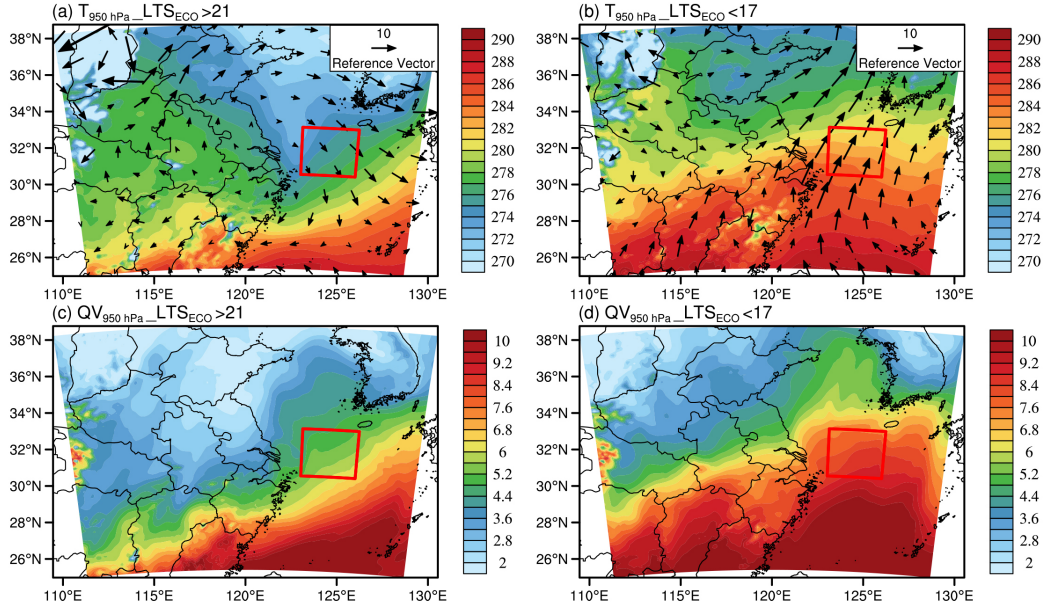

https://doi.org/10.5194/egusphere-2025-2555
Preprint. Discussion started: 15 July 2025


**Figure 1.** The 950 hPa temperature (a-b, in K), wind field (a-b, in $m \cdot s^{-1}$) and water vapor content (c-d, in $g \cdot m^{-3}$) during periods when the LTS in ECO (highlighted in red box) is high (>21, a and c) and low (<17, b and d), from the Control experiment.

Fig. 2 presents the temporal evolution of LTS, column-mean RH from the surface to 1300 m (this range captures over 97% of cloud droplets in both experiments and is used for all meteorological variables to better reflect their influence on ACI), $N_a$, and CLWP over ECO from the two experiments. For the meteorological field, significant variations in LTS and RH occurred during this period. As LTS increases, the aerosol-cloud processes over ECO transition from being driven by updraft to being dominated by cold advection. When LTS is low, ECO is primarily influenced by southerly winds (Fig. 1b), under which the lower atmosphere exhibits characteristics of warmth, moisture, and dominant updraft (Figs. 1 and S1). As LTS increases, ECO becomes dominated by dry, cold northwesterly winds (Fig. 1a), and both temperature and water vapor content in the lower atmosphere gradually decrease. Statistical analysis of grid points over ECO reveals a clear negative correlation between temperature and water vapor content at 950 hPa and LTS (correlation coefficients are -0.68 and -0.58, respectively, with p-values both less than 0.01). Accompanied by large-scale subsidence from the northwestern high-pressure system, a significant capping inversion forms at the top of the ECO boundary layer, strongly inhibiting updraft. However, with the rapid advection of northwestern low-level cold air, the lower atmosphere over ECO exhibits higher supersaturation than under low LTS (Fig. S1).

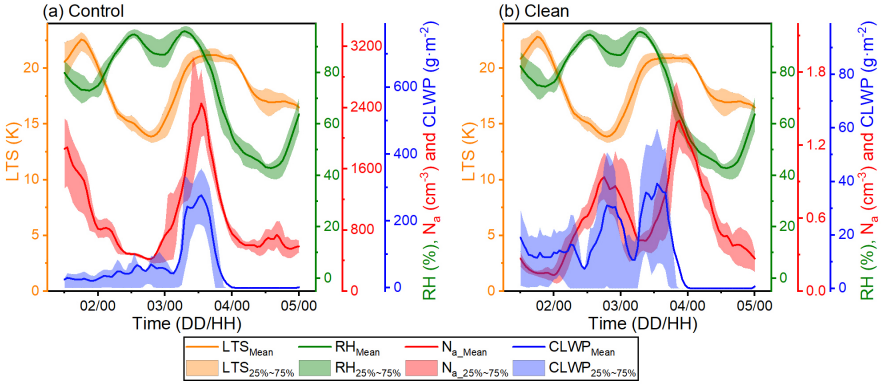


**Figure 2.** Variations in LTS, column-mean RH from the surface to 1300 m, $N_a$, and CLWP over ECO during the study period for the Control (a) and Clean (b) experiments.

For aerosols, the average $N_a$ under polluted and clean regimes differs by a factor of 1988. Under the polluted regime, ECO experiences high-pollution periods ($N_a$ > 2400 $cm^{-3}$, located along major continental aerosol transport pathway) and low-pollution periods ($N_a$ < 500 $cm^{-3}$, away from the pathway). Under the clean regime, aerosol concentrations over ECO also exhibit significant variability driven by marine emissions, with $N_a$ ranging from 0.13 $cm^{-3}$ to 1.4 $cm^{-3}$, differing by more than an order of magnitude. CLWP also exhibits pronounced variations in response to meteorological conditions and $N_a$.

This case encompasses typical variations in aerosols and meteorological fields. Analyzing it can deepen the understanding of (1) the impact of continental aerosols on marine liquid-phase clouds, (2) ACI under different pollution regimes, and (3) the influence of meteorological fields on ACI, offering great research value.

### 3.2 Experiment setup

In the simulations, nested grids with 48 vertical layers and horizontal resolutions of 12 km and 2.4 km are employed.

https://doi.org/10.5194/egusphere-2025-2555
Preprint. Discussion started: 15 July 2025


The outer domain (all colored areas in Fig. 1, including the parts obscured by the Reference Vector) is centered at (32°N, 120°E) with a grid number of 151×125, while the inner domain covers ECO with a grid number of 121×121. The simulation period is from 00:00 on Feb. 1, 2019, to 00:00 on Feb. 5, 2019, in UTC. The initial 12 hours are considered as model spin-up and are not included in the analysis. The model outputs once per hour.

Meteorological initial and boundary conditions are from the National Center for Environmental Prediction (NCEP) FNL reanalysis with a temporal and spatial resolution of 6 h and 0.25°, respectively (NCEP et al., 2015). Chemical initial and boundary conditions are from the Community Atmosphere Model with Chemistry (CAM-chem, Buchholz et al., 2019; Emmons et al., 2020). Anthropogenic emissions are from the Multi-resolution Emission Inventory for China (MEIC, 2016 version developed by Tsinghua University (Li et al., 2017; Zheng et al., 2018)). The radiative effects of aerosols and clouds are turned off to avoid their interference with the analysis of ACI. The model parameterization settings for the Control experiment are listed in Table 1. In the Clean experiment, continental emissions (including anthropogenic, dust, and biogenic sources) as well as aerosol and chemical initial and boundary conditions from CAM-Chem are disabled.

**Table 1.** Model parameterization settings for the Control experiment. "Number" refers to the WRF-Chem namelist switch.

| Process | Number | Name |
|---|---|---|
| Longwave radiation | 4 | RRTMG (Mlawer et al., 1997) |
| Shortwave radiation | 4 | RRTMG (Iacono et al., 2008) |
| Surface layer | 1 | MM5 Monin-Obukhov (Pahlow et al., 2001) |
| Land surface | 2 | Unified Noah (Chen et al., 2010) |
| Boundary layer | 1 | YSU (Shin et al., 2012) |
| Cumulus | 5 | Grell-3 (Grell et al., 2014) |
| Chemistry and aerosols | 9 | CBMZ and four-bin MOSAIC (Sha et al., 2022) |
| Photolysis | 2 | Fast-J (Wild et al., 2000) |
| Sea salt emission | 2 | MOSAIC/SORGAM (Fuentes et al., 2011) |
| Dust emission | 13 | GOCART (Zhao et al., 2010) |
| Biogenic emission | 3 | MEGAN (Guenther et al., 2006). |

In addition, the four-dimensional assimilation method is used in this study to improve the model's ability to simulate the meteorological field and thus enhance the model's ability to reproduce the factual aerosol-cloud scenario (Zhao et al., 2020; Hu et al., 2022). The assimilation uses observations of altitude, wind direction, wind speed, air pressure, temperature, and dew point, obtained from the NCEP operational global surface (NCEP et al., 2004) and upper air (Satellite Services Division et al., 2004) observation subsets.

### 3.3 Model evaluation

Multiple observational datasets are used in this study to evaluate the simulated meteorological fields, aerosols, clouds, and precipitation. The simulated cloud and precipitation in the inner domain are compared with the observations, while the simulated meteorological fields and aerosols in the outer domain are used for comparison due to limitations in observational data resolution and availability.

The vertical profiles of domain mean observed and simulated meteorological elements (Fig. 3) indicate that the simulations with and without assimilation reasonably reproduce the vertical variation of the observations. Assimilation generally has a positive impact on the meteorological field simulation, as evidenced by the comparison of the control

https://doi.org/10.5194/egusphere-2025-2555
Preprint. Discussion started: 15 July 2025


experiments with and without assimilation. Except for the dewpoint depression at 100 to 200 hPa and the zonal wind at 500 hPa, the means and uncertainties of the meteorological elements at various pressure levels with assimilation show higher agreement with the observations than without assimilation. Correlation analysis between observed and simulated data at each grid point (Fig. S2) also demonstrates the overall positive impact of assimilation, especially significantly improving the model's ability to simulate dewpoint depression (with the average correlation between simulated and observed dewpoint depression increasing by 16%), which effectively enhances the model's capability in aerosol-cloud simulation.

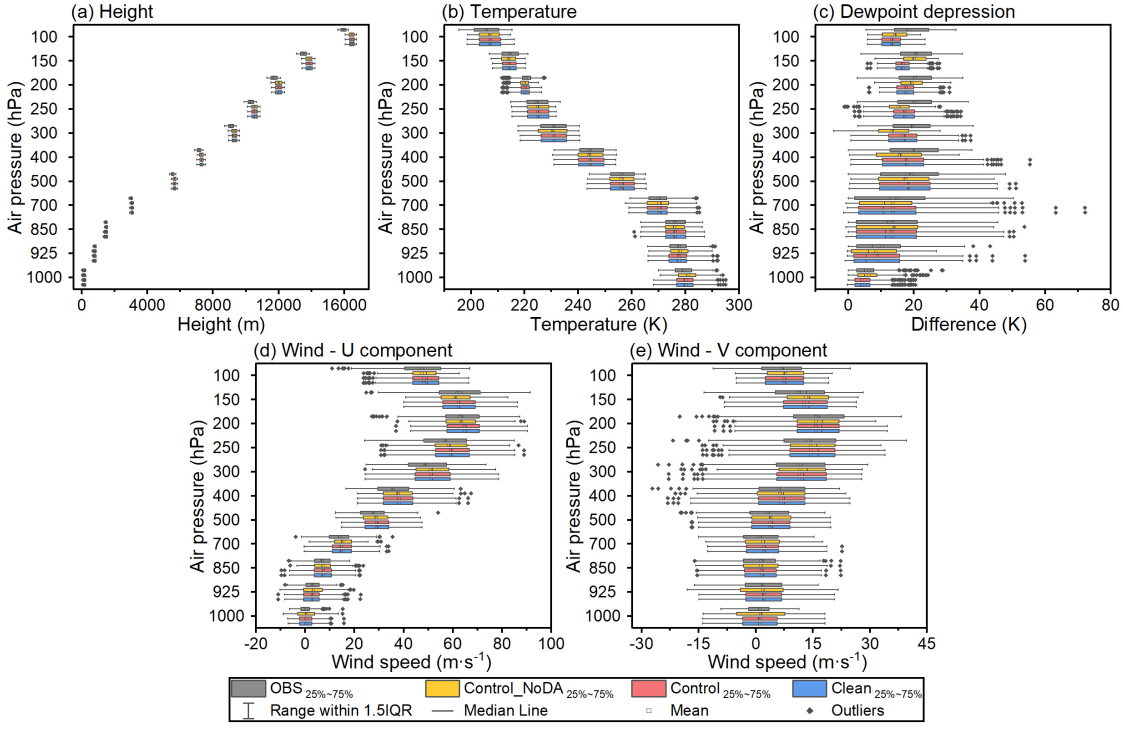


**Figure 3.** The observed (MICAPS, in black) and simulated (Control_NoDA, Control, and Clean—representing the Control experiment without assimilation, and the Control and Clean experiments with assimilation, shown in orange, red, and blue, respectively) height (a), temperature (b), dewpoint depression (c), and zonal (d) and meridional (e) winds of the outer domain at each pressure level, including the 25th to 75th percentile range, mean, median, range with 1.5 IQR (Interquartile Range), and outliers.

Supported by realistically reproduced meteorological fields, high-resolution emission data, and well-defined aerosol initial and boundary conditions, the model accurately captures the spatial distribution of observed AOD and near-surface $PM_{2.5}$ (Figs. 4a-f), with spatial correlations of 0.80 and 0.95 and NMBs of -13.22% and 6.78%, respectively. Although direct $PM_{2.5}$ observations are unavailable over ECO, the consistency between AOD, $PM_{2.5}$ from nearby areas, and the accuracy of wind field simulations suggests that the model can reasonably reproduce aerosol characteristics in this region. Compared to aerosol simulations, cloud and precipitation modeling remains more challenging due to uncertainties in microphysical processes (Figs. 4g-o). Clear discrepancies are found between simulated and observed cloud parameters in northeastern and southern ECO. However, the simulations remain highly correlated with observations, with correlation coefficients of 0.81 for $N_d$ and 0.72 for CLWP. The model captures the observed precipitation zones in northwestern ECO

https://doi.org/10.5194/egusphere-2025-2555
Preprint. Discussion started: 15 July 2025


and the southwest-northeast rainband, though slight spatial shifts result in a relatively low correlation (0.57) with observations. Overall, the model reproduces the spatial distributions of aerosols, clouds, and precipitation within an acceptable error range (±30%), and uncertainty statistics in Fig. S3 further support the consistency between simulations and observations. The evaluation provides a credible foundation for simulation-based analyses of aerosol–cloud interactions.

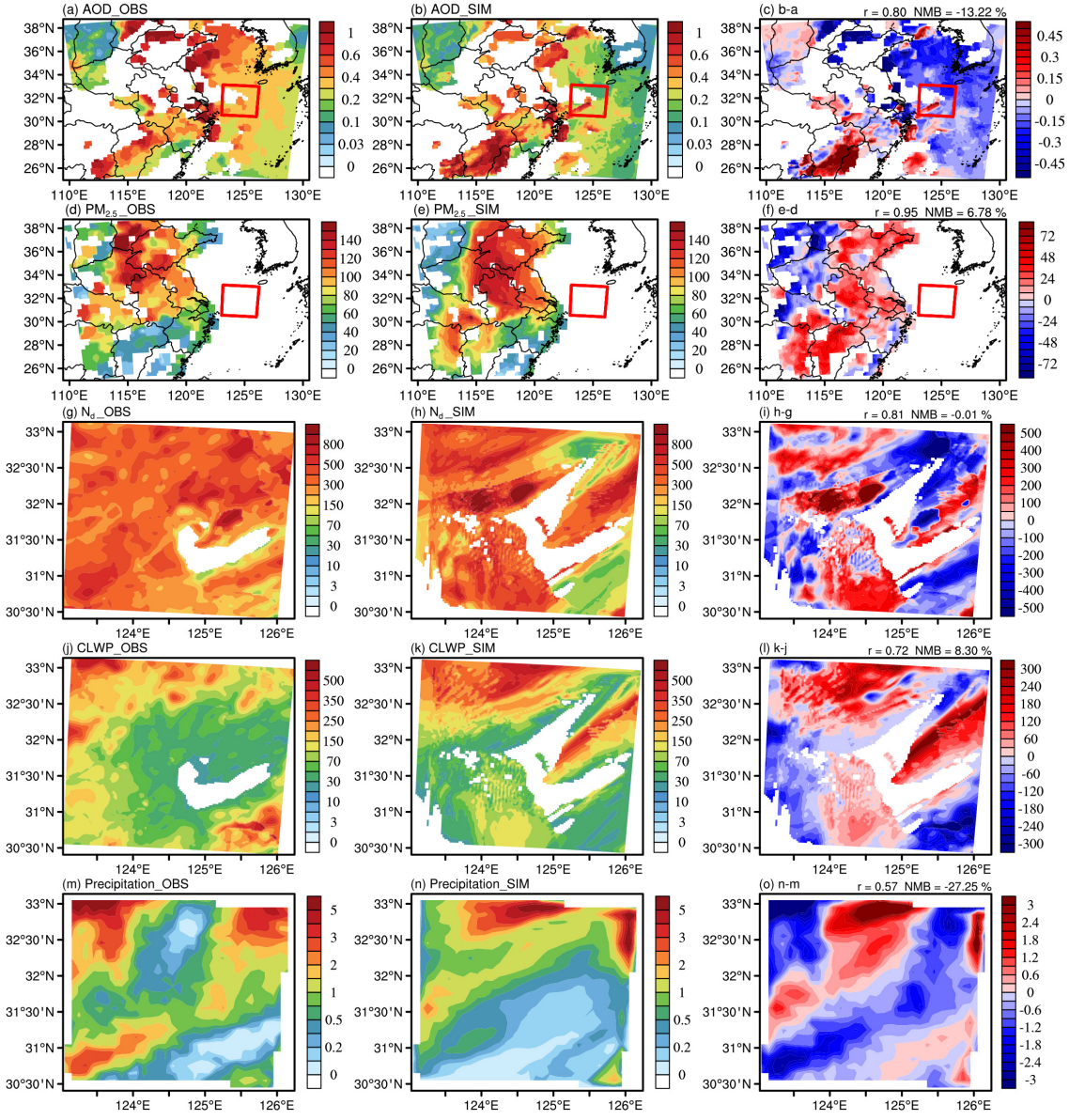


**Figure 4.** Distributions of observed (left column. AOD and cloud properties, near-surface $PM_{2.5}$, and precipitation from MODIS retrievals, near-surface observations, and IMERG, respectively) and simulated (middle column, from Control experiment) AOD (a-c), near-surface $PM_{2.5}$ (d-f, in $\mu g \cdot m^{-3}$), $N_d$ (g-i, in $cm^{-3}$), CLWP (j-l, in $g \cdot m^{-2}$), and cumulative precipitation (m-o, in mm) as well as the differences between simulations and observations (right column, r and NMB in the upper right corner represent the spatial correlation coefficient and normalized mean bias between simulation and

https://doi.org/10.5194/egusphere-2025-2555
Preprint. Discussion started: 15 July 2025


observation). Model output is shown only for columns where observations are available.

### 3.4 The robustness of the simulated signals

In this study, we analyze the sensitivity of ACI to meteorological conditions in different environments by comparing Control and Clean experiments. Two key challenges must be addressed to ensure the robustness of the simulated signals: (1) maintaining consistency in the meteorological fields between the two experiments, and (2) statistically demonstrating the robustness of the inter-experiment differences, specifically by showing that the differences between the two experiments are greater than the simulation error between the Control experiment and observations.

To address issue (1), we technically eliminate the perturbation to meteorological fields by disabling the radiative effects of aerosols and clouds. Additionally, four-dimensional data assimilation supports the consistency of the meteorological fields. The vertical profiles (Fig. 3) and the spatial distribution of inter-experiment correlations (Fig. S4) of meteorological parameters reveal highly consistent patterns and strong correlations (the correlation at every grid point exceeds 0.99, all pass the 99% significance test, and the average absolute NMB for all variables is only 0.06%), statistically confirming the consistency of meteorological fields between the two experiments.

To addressing issue (2), ideally, comprehensive observational data should be used to evaluate in detail the spatiotemporal distribution of simulation differences between the two experiments and the simulation errors between the Control experiment and observations. High-confidence data from segments where the former exceeds the latter should be used for analysis. However, due to the limited availability of observational data, particularly for aerosol and cloud parameters, which cover less than 10% of the simulated spatiotemporal range, the error assessment based on these observations cannot serve as the basis for selecting data for analysis. Therefore, issue (2) is addressed from the perspective of experimental design and statistical analysis of aerosol and cloud parameters. First, the only difference between the Control and Clean experiments is the containing of continental aerosols. According to the simulation results, the average aerosol number concentration in the two experiments differs by a factor of 1988, representing an extreme forcing scenario and providing a strong foundation for the analysis. This strong external perturbation inherently suggests that if aerosols have an impact on clouds and precipitation, it should be reflected in the simulation. Second, the statistical analysis of the uncertainty in aerosol and cloud parameters between the observations and simulations, shown in Fig. S3, indicates that the differences in aerosol and cloud parameters between the two experiments are much larger than those between the Control experiment and the observations. Due to the offsetting effects of aerosols on both enhancing and weakening precipitation (Figs. 5m-o), the 25%~75% range of the two experiments is similar. However, in the range with 1.5 IQR and outliers, the differences between the two experiments are comparable to the differences between the Control and observations, providing support for the significance of the results.

## 4 Results and discussion

### 4.1 Impact of continental aerosols on clouds and precipitation

Continental aerosols exert a substantial impact on liquid-phase clouds over ECO (Fig. 5) due to their vast quantity (reaching 1,988 times that of marine emissions). This leads to an average 248-fold increase in $N_d$, a 77.1% decrease in CER, and a 2.75-fold rise in CLWP across this region. Compared to their effects on clouds, the influence of continental aerosols on precipitation is more heterogeneous, with both enhancements and suppressions partially offsetting each other, resulting in an overall 6.9% increase in precipitation over ECO.

https://doi.org/10.5194/egusphere-2025-2555
Preprint. Discussion started: 15 July 2025


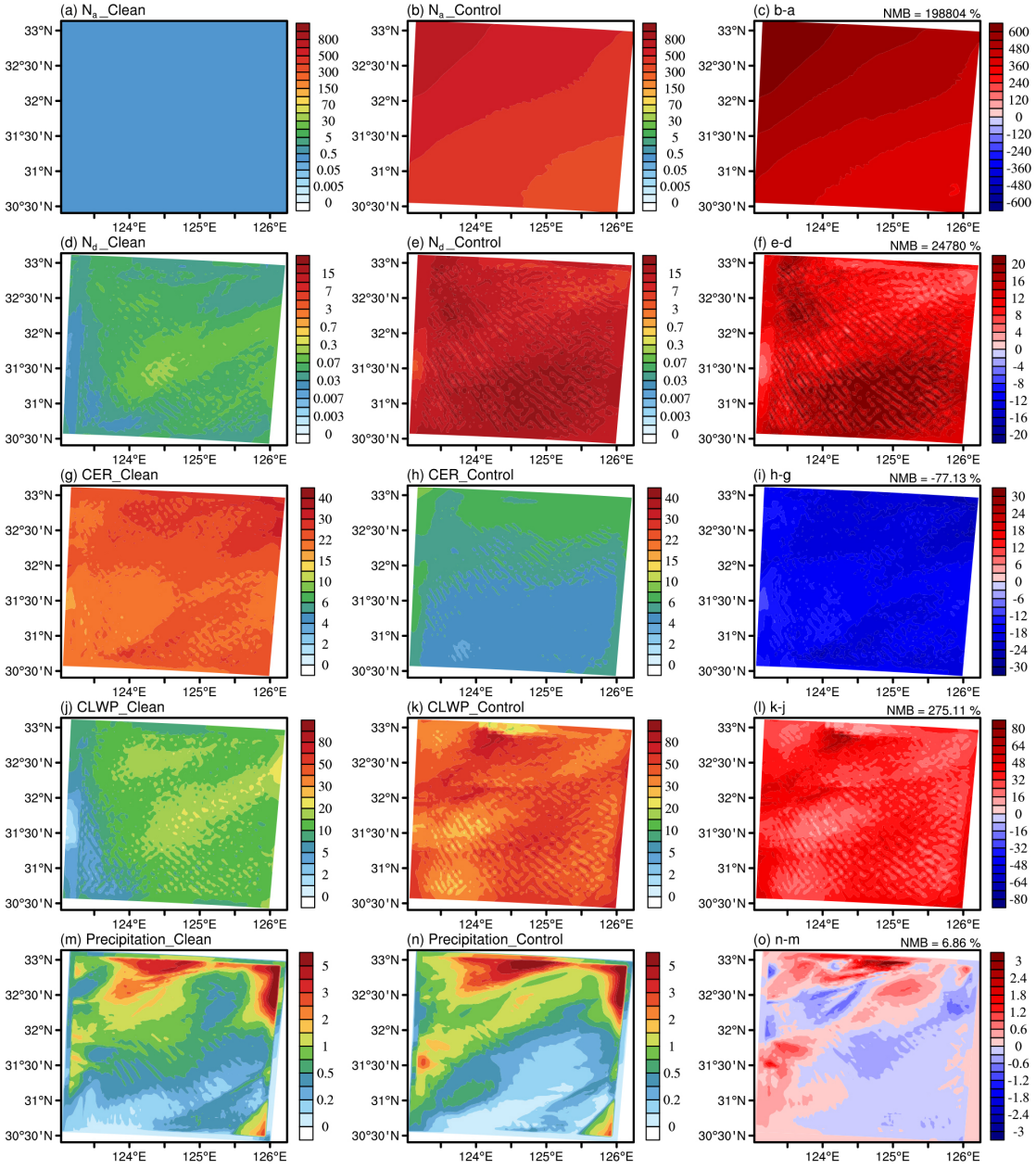


**Figure 5.** Column-mean $N_a$ (a-c, in $cm^{-3}$), in-cloud mean $N_d$ (d-f, in $cm^{-3}$), CER (g-i, in μm) and CLWP (j-l, in $g \cdot m^{-2}$), and accumulated precipitation (m-o, in mm) from the Clean (left column) and Control (middle column) experiments. The right column shows the differences between the two experiments (Control minus Clean). NMB in the top-right corner of each panel represents the relative change of Control compared to Clean.

Cloud development under both pollution regimes and the enhancing effect of continental aerosols on clouds exhibit regular variations with RH and LTS (Fig. 6). Since tests shown in Fig. S5 indicate that LTS and RH do not exhibit noticeable lagged effects on clouds at 1-, 3-, and 6-hour lag times in this case, lag analysis is not applied in this study. Between the

https://doi.org/10.5194/egusphere-2025-2555
Preprint. Discussion started: 15 July 2025


surface and 1300 m, where more than 97% of the cloud droplets in this case are located, supersaturation occurs mainly in humid environments with RH above 60% and increases with LTS. Except in a few weak clouds under relatively low RH conditions (<85%), where the reduction in droplet size due to continental aerosols intensifies evaporation and weakens the cloud, continental aerosols generally increase $N_d$ and CLWP across ECO. Both cloud processes in each experiment and the continental aerosol-induced enhancement of $N_d$ and CLWP strengthen with increasing LTS, similar to the behavior of supersaturation. This suggests that, in the winter case studied, cold advection plays a dominant role in cloud development compared to updraft. Additionally, we analyze the cloud lifetime effect induced by continental aerosols based on the occurrence frequency of liquid-phase clouds (defined as the total count of grid points where and when CLWP exceeds 1 $g \cdot m^{-2}$ and no ice-phase particles are present). The results (Figs. 6m–o) show that under relatively moist conditions (RH > 85%), continental aerosols extend cloud lifetime, with this effect first decreasing and then increasing with LTS. The extension is strongest when LTS is either low or high, corresponding to the most vigorous updrafts and cold advection, respectively. Under relatively dry conditions (RH < 85%), enhanced evaporation driven by aerosol-induced reductions in CER dominates, leading to accelerated cloud dissipation and shortened cloud lifetime.

https://doi.org/10.5194/egusphere-2025-2555
Preprint. Discussion started: 15 July 2025


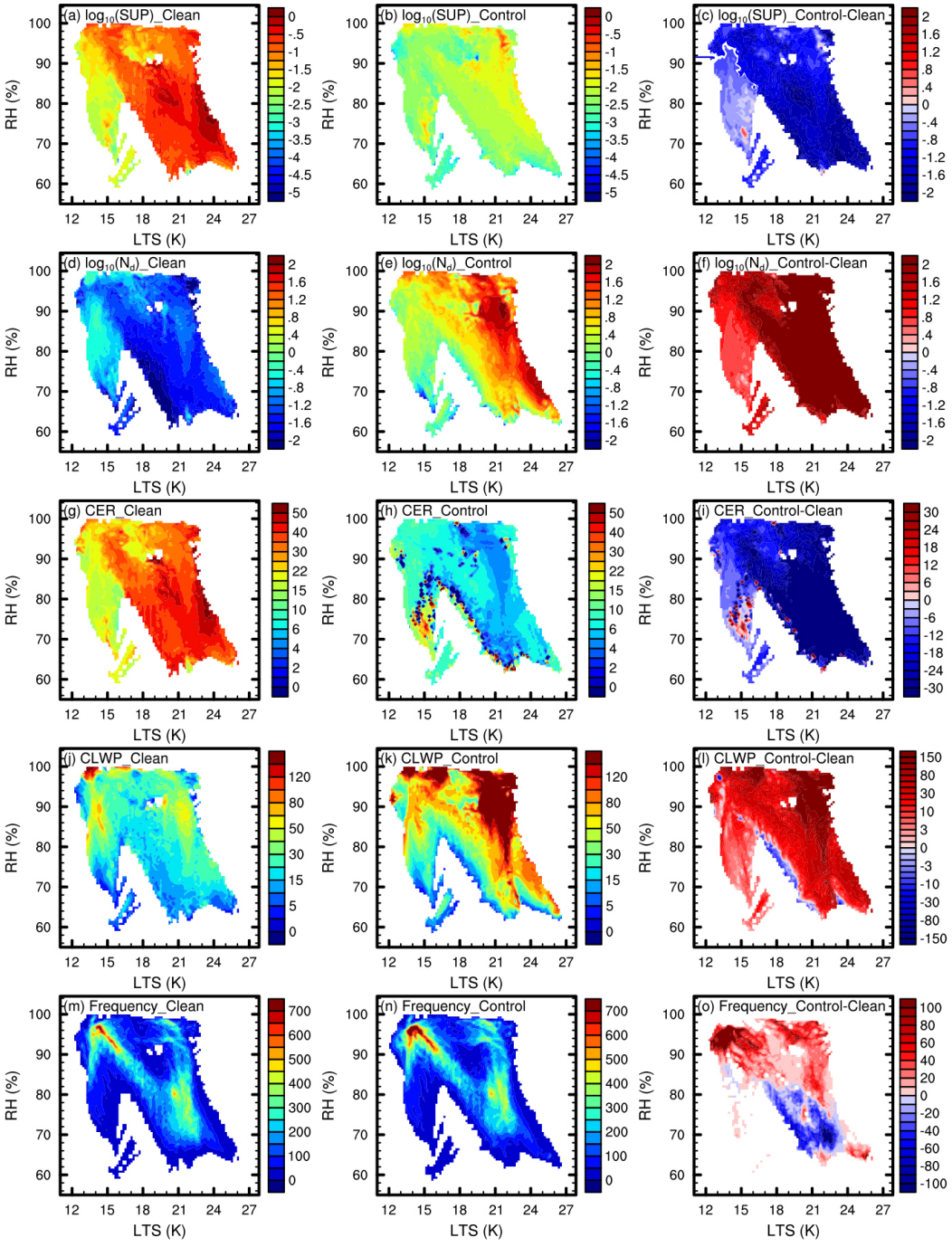


**Figure 6.** In-cloud mean supersaturation (a-c, in %) in base-10 logarithms, $N_d$ (d-f, in $cm^{-3}$) in base-10 logarithms, CER (g-i, in μm), and CLWP (j-l, in $g \cdot m^{-2}$), as well as the frequency of liquid-phase cloud (m-o) variations with RH and LTS, are presented for the Clean (left column) and Control (middle column) experiments, along with the difference between them (Control minus Clean, right column) during the simulation period. Supersaturation and RH are column-mean values from the surface to 1300 m. All liquid-phase cloud samples with a CLWP greater than 1 $g \cdot m^{-2}$ and no ice-phase particles

https://doi.org/10.5194/egusphere-2025-2555
Preprint. Discussion started: 15 July 2025


throughout the column are included. Samples are binned into 100 × 100 bins based on horizontal and vertical coordinates. In the figure, frequency represents the sum of samples within each bin, while the others represent the average of samples within each bin.

The variations of precipitation parameters, including raindrop number concentration ($N_r$), rainwater path (RWP), and hourly precipitation, with RH and LTS are shown in Fig. 7. Similar to cloud parameters, both $N_r$ and RWP increase with LTS in both experiments. Continental aerosols generally suppress precipitation by reducing droplet size, but instances of precipitation enhancement are also observed. Increases in $N_r$ and RWP mainly occur under high-humidity conditions (RH > 90%), while the LTS conditions linked to increased precipitation appear relatively irregular. The effects of continental aerosols on $N_r$ and RWP are highly consistent. Due to differences in raindrop size and vertical position, the hourly precipitation generally aligns with changes in $N_r$ and RWP, but exhibits discrepancies in some details. Compared to precipitation, which has a lagged response, $N_r$ and RWP provide more immediate and accurate tracking of the aerosol-cloud-precipitation processes. Subsequent analyses of precipitation therefore focus on $N_r$ and RWP.

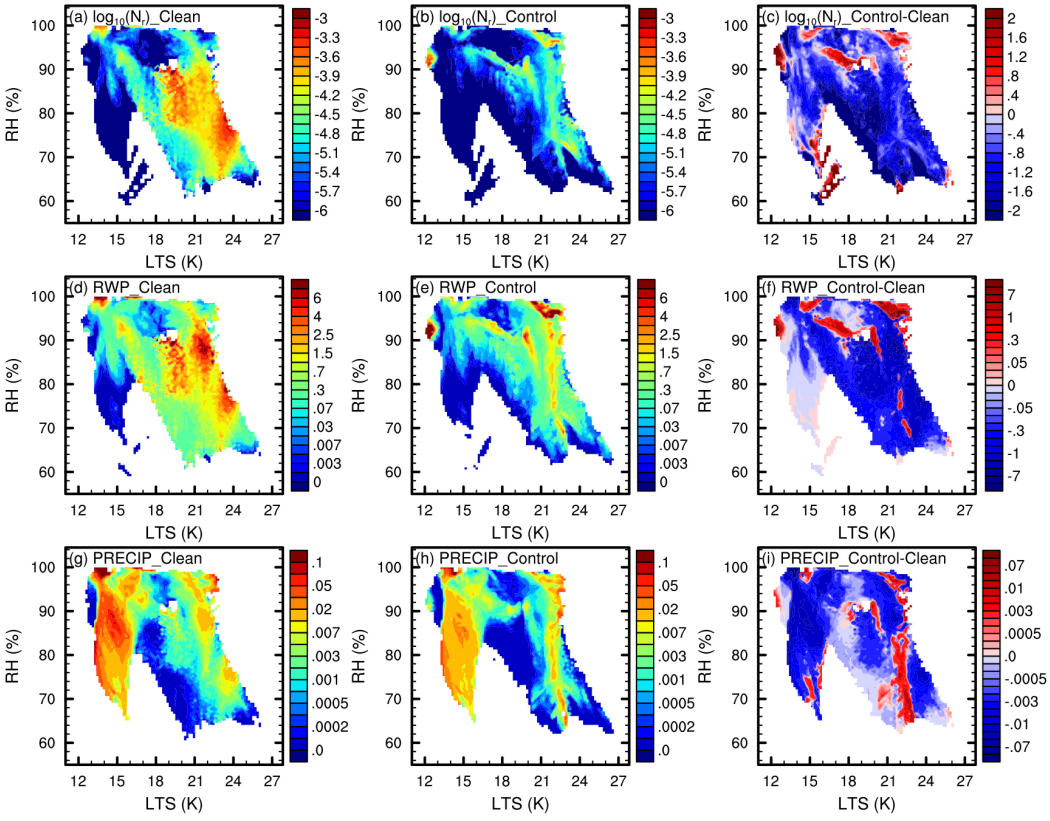


**Figure 7.** The mean $N_r$ (a-c, in $cm^{-3}$), RWP (d-f, in $g \cdot m^{-2}$), and hourly precipitation (g-i, in $mm \cdot h^{-1}$) variations with RH and LTS, are presented for the Clean (left column) and Control (middle column) experiments, along with the difference between them (Control minus Clean, right column) during the simulation period. The data processing method is the same as that used in Fig. 6.

We analyze samples with enhanced and reduced precipitation under the influence of continental aerosols (selecting samples with RWP increases and decreases greater than 0.001 $g \cdot m^{-2}$) to further understand the mechanism of continental

https://doi.org/10.5194/egusphere-2025-2555
Preprint. Discussion started: 15 July 2025


aerosol effects on precipitation (Fig. 8). For the precipitation reduction samples, the differences in $N_r$ and RWP between the two experiments at high levels (1600~4000 m) are small. However, at the low levels (around 500 m) where the majority of cloud droplets are located, the decrease in CER significantly suppresses precipitation, causing it to reduce by an order of magnitude. For the precipitation enhancement samples, under the influence of continental aerosols, the column-mean $N_d$ is 2.64 times higher than in the precipitation reduction samples. At low levels, the collision and coalescence of numerous cloud droplets produce more large droplets (as indicated by the 75th percentile value of CER) and raindrops, while stronger vertical development of clouds at high levels also leads to a significant increase in $N_r$ and RWP.

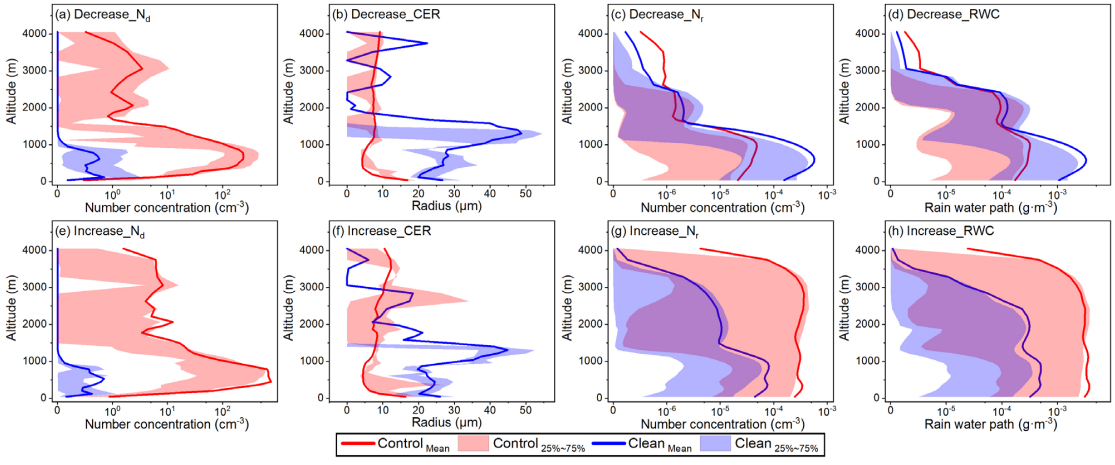


**Figure 8.** Vertical profiles of the average $N_d$ (a and e), CER (b and f), $N_r$ (c and g), and RWC (d and h) for precipitation reduction (a-d) and enhancement (e-h) samples under the influence of continental aerosols.

### 4.2 ACI under different pollution regimes

In Section 4.1, by examining the variation of cloud parameters with LTS and RH, we gain an overall understanding of how liquid-phase clouds under the two pollution regimes and the influence of continental aerosols respond to meteorological conditions. However, this apparent cloud response also contains embedded signals of ACI induced by aerosol variability within each regime. In this section, we further explore the sensitivity of ACI to meteorological conditions by analyzing cloud responses to meteorological conditions at varying $N_a$ levels under different regimes.

In addition to cloud properties such as CER, CLWP, and RWP, we use ratios including $N_d/N_a$, CLWP/$N_a$, and RWP/$N_a$ to characterize activation efficiency, as well as the response rates of CLWP and RWP to $N_a$ (Fig. 9). The variation of clouds with LTS reflects the dynamical influence of meteorological conditions on ACI. Under the clean regime, aerosol activation efficiency shows little sensitivity to changes in LTS or $N_a$ due to the very low aerosol number dominated by large particles from natural emissions (Fig. 10a), which maintains cloud processes in an aerosol-limited state. As $N_a$ increases, aerosols continue to activate with high efficiency to form cloud droplets, thereby promoting an increase in CLWP. However, in the aerosol-limited state, the weak role of collision-coalescence and the dominance of condensation cause the CER reduction induced by increased $N_a$ to suppress precipitation, while the growth rate of CLWP gradually slows.

https://doi.org/10.5194/egusphere-2025-2555
Preprint. Discussion started: 15 July 2025


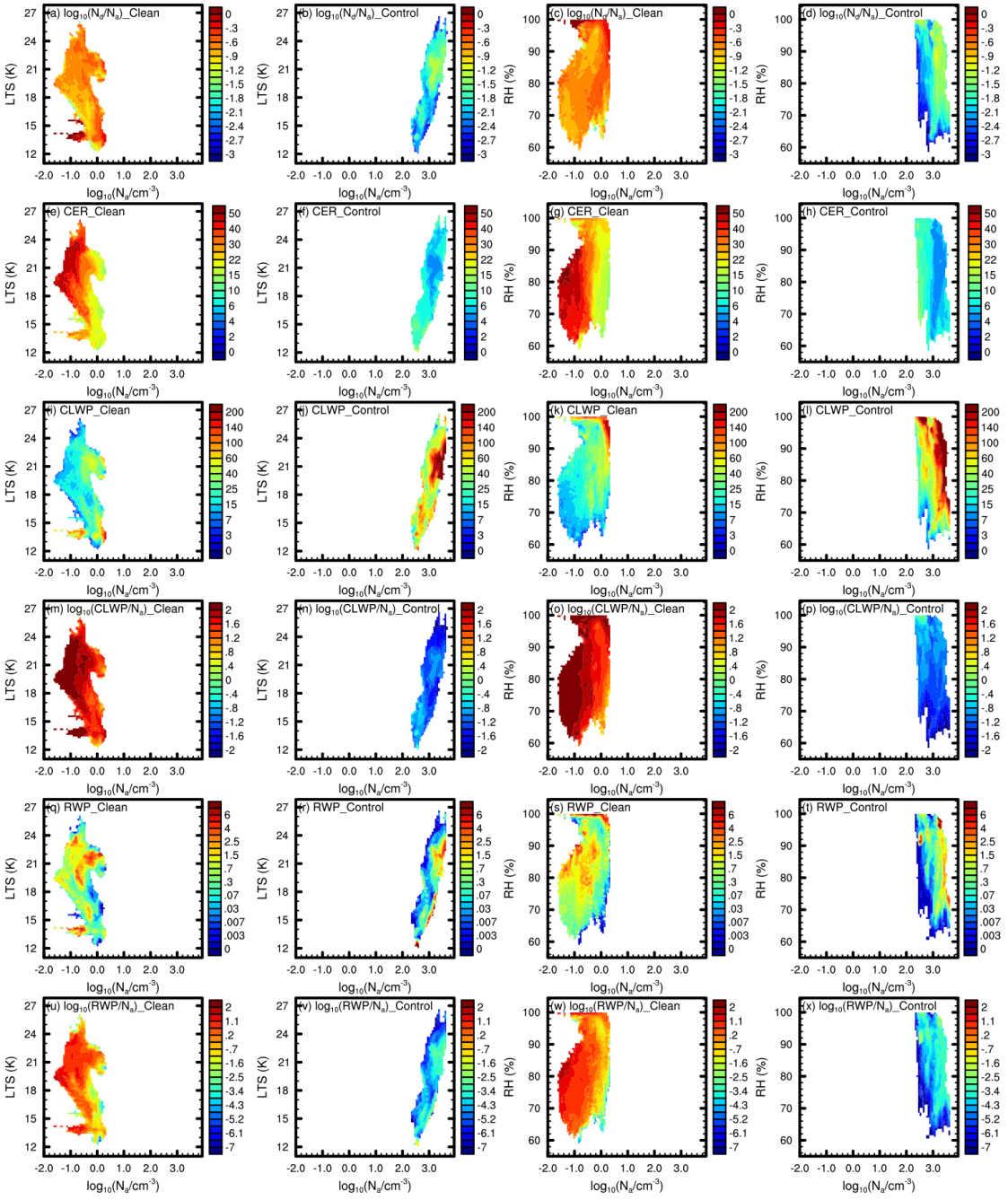


**Figure 9.** Variations of in-cloud mean $N_d/N_a$ (a-d, in $cm^{-3}\cdot cm^3$) in base-10 logarithms, CER (e-h, in μm), CLWP (i-l, in $g\cdot m^{-2}$), CLWP/$N_a$ (m-p, in $g\cdot m^{-2}\cdot cm^3$) in base-10 logarithms, RWP (q-t, in $g\cdot m^{-2}$), and RWP/$N_a$ (u-x, in $g\cdot m^{-2}\cdot cm^3$) in base-10 logarithms with meteorological conditions (LTS, left two columns, and RH, right two columns) and $N_a$ in base-10 logarithms for the Clean (first and third columns) and Control (second and fourth columns) experiments. The data processing method is the same as that used in Fig. 6.

https://doi.org/10.5194/egusphere-2025-2555
Preprint. Discussion started: 15 July 2025


The influence of LTS is more pronounced in the polluted regime, which contains a large number of aerosols dominated by small particles (Fig. 10a). Statistical analysis reveals a significant negative correlation between the column-mean $N_a$ and temperature at 950 hPa over ECO ($r = -0.58$, $p < 0.01$), indicating that higher $N_a$ during the winter monsoon is associated with stronger cold advection. Under low LTS, increases in $N_a$ coincide with weakened updrafts, whereas under high LTS, increases in $N_a$ correspond to intensified cold advection. This leads to a decrease in activation efficiency and CLWP growth rate with $N_a$ under low LTS, and an increase under high LTS. Moreover, as CER decreases and CLWP increases, RWP strengthens under the polluted regime, compared to its weakening under the clean regime, reflecting the dominant role of collision-coalescence among numerous small cloud droplets (Fig. 10b).

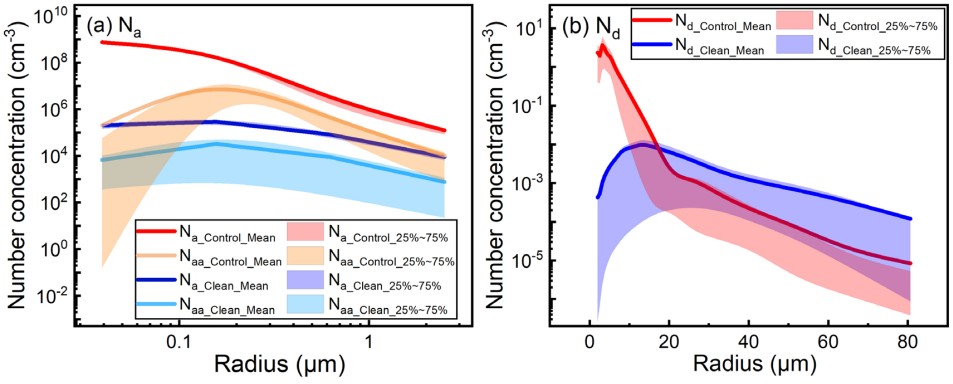


**Figure 10.** In-cloud mean aerosol (a, $N_a$ as total aerosol number concentration, $N_{aa}$ as activated aerosol number concentration) and droplet (b) size distribution in the Control and Clean experiments.

The variation of clouds with RH reflects the influence of meteorological conditions from the perspective of water vapor supply (right two columns in Fig. 9). Under the clean regime, clouds show much stronger sensitivity to RH than to LTS, with activation efficiency, CER, CLWP, and RWP all steadily increasing with RH. Compared to the clean regime, the polluted regime, characterized by abundant aerosols and a water-vapor-limited environment, exhibits greater cloud sensitivity to RH. Additionally, from the RH perspective, cloud parameters vary with $N_a$ in a manner similar to that observed under high LTS, further highlighting the dominant role of cold advection in this winter case.

The assessment of the sensitivity of ACI to meteorological conditions based on RH and LTS primarily focuses on the influence of thermodynamic conditions. However, due to the delayed responses of clouds to thermodynamic conditions, along with disturbances from small-scale physical processes, the response of ACI to RH and LTS exhibits discontinuities and uncertainties under some conditions. We further investigate the sensitivity of ACI to meteorological conditions based on supersaturation (column-mean from the surface to 1300 m), which serves as a more immediate and responsive indicator (Fig. 11). Cloud parameters in both regimes exhibit strong sensitivity to supersaturation. Under the clean regime, $N_d$, CER, CLWP, and RWP all increase with supersaturation. Under this aerosol-limited regime, cloud parameters are also sensitive to aerosols. As $N_a$ increases, $N_d$, CLWP, and RWP generally show consistent increases, while CER correspondingly decreases. A notable deviation from this overall trend occurs when $N_a$ falls within the range of $10^{-0.8}$ to $10^{-0.4}$ $cm^{-3}$ and supersaturation is below 0.1%, where RWP shows a relatively high-value band. This is because, within this $N_a$ range, $N_d$ increases with $N_a$, while CER remains relatively high (approaching 40 μm even under low supersaturation). When $N_a$ exceeds $10^{-0.4}$ $cm^{-3}$, CER under low supersaturation rapidly decreases to around 15 μm, and high RWP appear only under high supersaturation.

https://doi.org/10.5194/egusphere-2025-2555
Preprint. Discussion started: 15 July 2025


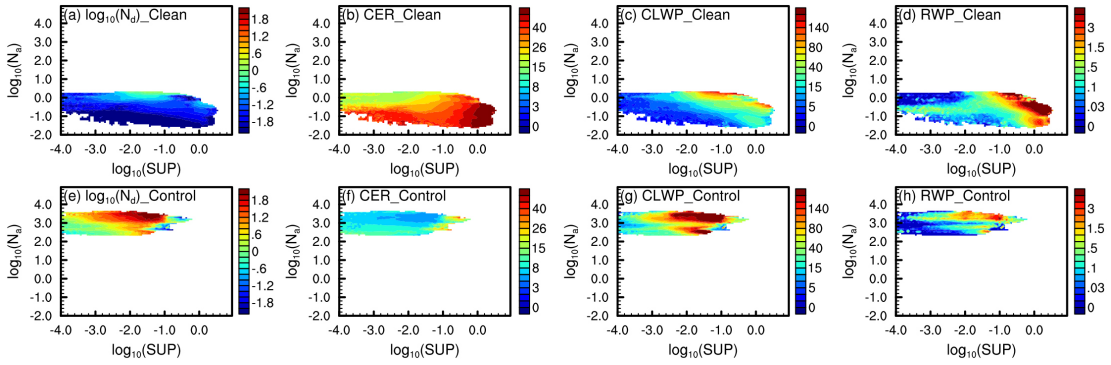


**Figure 11.** Variation of in-cloud mean $N_d$ (a and e, in $cm^{-3}$) in base-10 logarithms, CER (b and f, in μm), CLWP (c and g, in $g \cdot m^{-2}$), and RWP (d and h, in $g \cdot m^{-2}$) with $N_a$ (in $cm^{-3}$) and supersaturation (SUP, in %) in base-10 logarithms for the Sen (a-d) and Control (e-h) experiments during the simulation period. The data processing method is the same as that used in Fig. 6.

In clear contrast to the clean regime, $N_d$, CLWP, and RWP under the polluted regime exhibit non-monotonic responses to both supersaturation and $N_a$: they initially increase and then decrease with supersaturation, and show a decrease followed by an increase with $N_a$. At sub-moderate supersaturation levels (<$10^{-0.9}$%), increasing supersaturation promotes aerosol activation, resulting in higher $N_d$, CLWP, and RWP. However, as supersaturation continues to rise, many droplets grow to moderate size. Their stronger competition for water vapor relative to small droplets, along with the rapid evaporation of the latter, leads to a significant reduction in the number of small droplets. This weakens the collision-coalescence process and ultimately inhibits the formation of large droplets. At high supersaturation (>$10^{-0.8}$ %), although CER increases, only moderate-sized droplets increase, while both raindrop and small droplets decrease significantly compared to moderate ($10^{-2.0}$ to $10^{-0.9}$ %) supersaturation (as shown in Fig. 12), resulting in reductions in $N_d$, CLWP, and RWP. In comparison, the non-monotonic response of cloud parameters to $N_a$, consistent with the results in Fig. 9, arises from the shift in cloud processes from updraft dominance to cold advection dominance as $N_a$ increases. At moderate $N_a$, both updrafts and cold advection are weak, resulting in weakened clouds. Moreover, due to minimal precipitation during the study period (maximum and mean hourly precipitation for all liquid-phase cloud samples in the two experiments are 0.25 and 0.004 $mm \cdot h^{-1}$, respectively), precipitation closely follows changes in CLWP and does not significantly feedback on cloud processes.

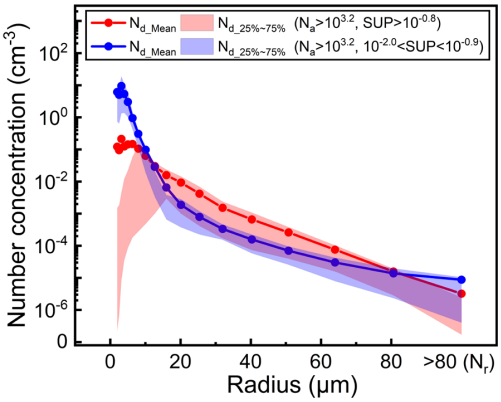


**Figure 12.** In-cloud cloud droplet and raindrop (droplet with a radius greater than 80 μm) spectral distributions (mean and

https://doi.org/10.5194/egusphere-2025-2555
Preprint. Discussion started: 15 July 2025


25th to 75th percentile range) in medium ($10^{-2.0}$ to $10^{-0.9}$ %, blue line) and high supersaturation (>$10^{-0.8}$ %, red line) environments under high $N_a$ (>$10^{3.2}$ $cm^{-3}$) during the simulation period.

## 4 Summary and conclusion

Large uncertainty remains in ACI due to its complex physical and dynamical mechanisms. Many studies have been conducted to examine the mechanisms of ACI and have found that the aerosol-cloud relationship varies significantly under different meteorological conditions. In this study, WRF-Chem-SBM model, which couples spectral bin cloud microphysics with an online aerosol module, is used to simulate a wintertime liquid-phase cloud case over ECO. The model's high-precision simulation of aerosol-cloud processes, the case featuring rich variability in meteorological, aerosol, and cloud parameters, the comparison between the Control experiment (representing a polluted regime with both continental and marine aerosols) and the Clean experiment (representing a clean regime with only marine aerosols), and the isolation of radiative effect interference through model configuration collectively support an in-depth understanding of the sensitivity of ACI to meteorological conditions.

To ensure the reliability of the simulation results and quantify the impact of four-dimensional data assimilation, we evaluate the simulations using multi-source observational data, including meteorological fields, aerosols, clouds, and precipitation. The evaluation indicates that data assimilation generally improves meteorological simulations, with particularly notable improvements in dewpoint depression (with the average correlation between simulated and observed dewpoint depression increasing by 16%). This effectively enhances the model's ability to simulate ACI. With support of assimilation, the model (Control experiment) well reproduces the values and distributions of meteorological fields, aerosols, and cloud parameters, with correlation coefficients above 0.72 and errors within ±13.3% relative to observations. The model reasonably reproduces precipitation amounts and spatial distribution of precipitation bands. However, due to slight positional discrepancies between simulated and observed rainbands, the agreement (r = 0.57, NMB = –27.3%) between simulation and observation is lower than for other parameters. Evaluation of the spatial distribution and uncertainties in simulations and observations indicates that the model reproduces meteorological fields, aerosols, clouds, and precipitation within acceptable error ranges, thereby supporting the reliability of the results. The consistency of meteorological fields between the Control and Clean experiments, along with the inter-experiment differences in aerosol–cloud interactions, further demonstrate the robustness of the simulated signals.

The simulation results reveal the substantial impact of continental aerosols on liquid-phase clouds over ECO, leading to a 248-fold increase in $N_d$, a 77.1% decrease in CER, and a 2.75-fold rise in CLWP on average. This impact and cloud processes under both polluted and clean regimes are enhanced with increasing LTS, which highlights the dominant role of cold advection over updraft in the context of the winter monsoon. Continental aerosols extend cloud lifetime in moist environments, with this enhancement strongest under low and high LTS conditions, where updraft and cold advection are most vigorous. In dry environments, however, the aerosols shorten cloud lifetime by intensifying evaporation. Moreover, continental aerosols exhibit both enhancing and suppressing effects on precipitation over ECO, but these effects do not show clear sensitivity to RH or LTS. Instead, the difference between enhanced and suppressed precipitation samples lies primarily in the intensity of cloud processes, with the former exhibiting an average $N_d$ 2.64 times higher than the latter. In weak cloud processes, aerosol-induced increases in $N_d$ and reductions in CER significantly suppress precipitation, whereas in intense cloud processes, enhanced vertical development and vigorous collision-coalescence among numerous droplets lead to increased precipitation.

Building on the overall analysis of cloud process variations with LTS and RH, we further explore the sensitivity of ACI to meteorological conditions by analyzing cloud responses to meteorological factors at varying $N_a$ levels under different regimes. The variation with LTS reveals the sensitivity of ACI to meteorological conditions from a dynamical

https://doi.org/10.5194/egusphere-2025-2555
Preprint. Discussion started: 15 July 2025


perspective. In the aerosol-limited clean regime, aerosol activation efficiency shows no clear sensitivity to LTS. As $N_a$ increases, aerosols still activate efficiently to form cloud droplets, leading to an increase in CLWP. However, under this aerosol-limited conditions, the weak role of collision-coalescence and the dominance of condensation suppress precipitation as CER decreases, while the growth rate of CLWP also slows with the reduction of CER. Under the polluted regime, characterized by abundant aerosols, cloud parameters exhibit strong sensitivity to LTS and show contrasting responses to $N_a$ under different dynamical conditions. Furthermore, unlike the clean regime where RWP decreases with CLWP, under the polluted regime RWP increases with CLWP, indicating the dominant role of collision-coalescence under this regime. Cloud processes under both clean and polluted regimes show clear sensitivity to RH, with the water-vapor-limited polluted regime exhibiting higher sensitivity. Additionally, from the RH perspective, cloud parameters vary with $N_a$ in a manner similar to that observed under high LTS, further emphasizing the dominant role of cold advection in this winter case.

We further investigate the sensitivity of ACI to meteorological conditions based on supersaturation, which serves as a more immediate and responsive indicator. Clouds in both regimes exhibit high sensitivity to supersaturation. Under the clean regime, $N_d$, CER, CLWP, and RWP all increase with supersaturation, and cloud parameters are also sensitive to aerosols due to the aerosol-limited state. Under the polluted regime, the initial decrease followed by an increase in cloud parameters with $N_a$, and their increase followed by a decrease with supersaturation, respectively reflect the influences of atmospheric dynamical conditions and collision-coalescence processes.

In this study, we build on existing theories of ACI and employ high-precision simulations of short-term processes to analyze their sensitivity to meteorological conditions, thereby helping to reduce uncertainties in ACI. However, statistical analyses based on small samples cannot conclusively demonstrate the existence of universal conditions. Given current computational limitations, we can only choose between high-precision small samples and low-precision large samples. In future research, combining this study with analyses of large sample observations or coarse-resolution simulations will be more beneficial in advancing the understanding of ACI.

***Code availability.*** The WRF-Chem model code can be downloaded from https://www2.mmm.ucar.edu/wrf/users/download/get_sources.html (University Corporation for Atmospheric Research, 2024). The WRF-Chem–SBM model code can be obtained by contacting Jiwen Fan (fanj@anl.gov) of Argonne National Laboratory.

***Data availability.*** The namelist file and output of the model can be downloaded from https://doi.org/10.5281/zenodo.15508465 (Zhao, 2025). NCEP data sets (https://doi.org/10.5065/39C5-Z211, Satellite Services Division et al., 2004; https://doi.org/10.5065/4F4P-E398, NCEP et al., 2004; https://doi.org/10.5065/D65Q4T4Z, NCEP et al., 2015), CAM-chem model output (https://doi.org/10.5065/NMP7-EP60, Buchholz et al., 2019), MICAPS meteorological fields (http://www.nmc.cn, National Meteorological Centre of China, 2009), near-surface $PM_{2.5}$ observations (https://air.cnemc.cn:18007, China National Environmental Monitoring Center, 2023), IMERG precipitation (https://doi.org/10.5067/GPM/IMERGDF/DAY/06, Huffman et al., 2019), and MODIS aerosol (https://doi.org/10.5067/MODIS/MOD04_L2.061, Levy et al., 2015) and cloud (https://doi.org/10.5067/MODIS/MOD06_L2.061, Platnick et al., 2015) data can be accessed from the corresponding websites or references.

***Author contributions.*** JZ and XM designed and conducted the model experiments, analyzed the results, and wrote the paper. XM developed the project idea and supervised the project. XM and JQ proposed scientific suggestions and revised the paper. TY collected and processed the data.

***Competing interests.*** One of the (co-)authors is a member of the editorial board of Atmospheric Chemistry and Physics,

https://doi.org/10.5194/egusphere-2025-2555
Preprint. Discussion started: 15 July 2025


and the authors have no other competing interests to declare.

***Acknowledgements.*** The numerical calculationsin this paper were conducted in the High-Performance Computing Center of Nanjing University of Information Science & Technology. We express our gratitude to Dr. Jiwen Fan of Argonne National Laboratory for providing the code for the WRF-Chem–SBM model. We are grateful to the National Aeronautics and Space Administration, the National Centers for Environmental Prediction, the MEIC support team, the Chinese National Meteorological Center, and the China National Environmental Monitoring Center for providing the MODIS and GPM data, FNL and observation subsets, MEIC emission inventory, MICAPS data, and $PM_{2.5}$ data, respectively.

***Financial support.*** This research has been supported by the Second Tibetan Plateau Scientific Expedition and Research program (grant no. 2019QZKK0103), the National Natural Science Foundation of China (grant nos. 42061134009 and 41975002), the China Scholarship Council program (grant no. 202309040034), and the Postgraduate Research and Practice Innovation Program of Jiangsu Province (grant no. KYCX22_1151).

## References

Albrecht, B. A.: Aerosols, cloud microphysics, and fractional cloudiness, Science, 245, 1227-1230, https://doi.org/10.1126/science.245.4923.1227, 1989.

Andersen, H., Cermak, J., Fuchs, J., Knutti, R., and Lohmann, U.: Understanding the drivers of marine liquid-water cloud occurrence and properties with global observations using neural networks, Atmos. Chem. Phys., 17, 9535-9546, https://doi.org/10.5194/acp-17-9535-2017, 2017.

Anwar, K., Alam, K., Liu, Y., Huang, Z., Huang, J., and Liu, Y.: Analysis of aerosol cloud interactions with a consistent signal of meteorology and other influencing parameters, Atmos. Res., 275, 106241, https://doi.org/10.1016/j.atmosres.2022.106241, 2022.

Arola, A., Lipponen, A., Kolmonen, P., Virtanen, T. H., Bellouin, N., Grosvenor, D. P., Gryspeerdt, E., Quaas, J., and Kokkola, H.: Aerosol effects on clouds are concealed by natural cloud heterogeneity and satellite retrieval errors, Nat. Commun., 13, 1-8, https://doi.org/10.1038/s41467-022-34948-5, 2022.

Brenguier, J.-L., Pawlowska, H., Schüller, L., Preusker, R., Fischer, J., and Fouquart, Y.: Radiative properties of boundary layer clouds: Droplet effective radius versus number concentration, J. Atmos. Sci., 57, 803-821, https://doi.org/10.1175/1520-0469(2000)057<0803:RPOBLC>2.0.CO;2, 2000.

Buchholz, R. R., Emmons, L. K., Tilmes, S., and The CESM2 Development Team: CESM2.1/CAM-chem Instantaneous Output for Boundary Conditions, UCAR/NCAR – Atmospheric Chemistry Observations and Modeling Laboratory [data set], https://doi.org/10.5065/NMP7-EP60, 2019.

Chang, C., Chen, W., and Chen, Y.: Susceptibility of East Asian Marine Warm Clouds to Aerosols in Winter and Spring from Co-Located A-Train Satellite Observations, Remote Sens., 13, 5179, https://doi.org/10.3390/rs13245179, 2021.

Chen, Y., Xue, L., Lebo, Z., Wang, H., Rasmussen, R., and Seinfeld, J.: A comprehensive numerical study of aerosol-cloud-precipitation interactions in marine stratocumulus, Atmos. Chem. Phys., 11, 9749-9769, https://doi.org/10.5194/acp-11-9749-2011, 2011.

Chen, Y., Christensen, M., Stephens, G., and Seinfeld, J.: Satellite-based estimate of global aerosol–cloud radiative forcing by marine warm clouds, Nat. Geosci., 7, 643-646, https://doi.org/10.1038/ngeo2214, 2014.

Chen, Y. Y., Yang, K., Zhou, D. G., Qin, J., and Guo, X. F.: Improving the Noah Land Surface Model in Arid Regions with an Appropriate Parameterization of the Thermal Roughness Length, J. Hydrometeorol., 11, 995-1006,

https://doi.org/10.5194/egusphere-2025-2555
Preprint. Discussion started: 15 July 2025


https://doi.org/10.1175/2010jhm1185.1, 2010.

China National Environmental Monitoring Center: National Urban Air Quality Real-time Publishing Platform, https://air.cnemc.cn:18007 (last access: 12 January 2025), 2023.

Dagan, G., Yeheskel, N., and Williams, A. I. L.: Radiative forcing from aerosol–cloud interactions enhanced by large-scale circulation adjustments, Nat. Geosci., 16, 1092-1098, https://doi.org/10.1038/s41561-023-01319-8, 2023.

Emmons, L. K., Schwantes, R. H., Orlando, J. J., Tyndall, G., Kinnison, D., Lamarque, J. F., Marsh, D., Mills, M. J., Tilmes, S., and Bardeen, C.: The chemistry mechanism in the community earth system model version 2 (CESM2), J. Adv. Model. Earth Syst., 12, e2019MS001882, https://doi.org/10.1029/2019MS001882, 2020.

Fuentes, E., Coe, H., Green, D., and McFiggans, G.: On the impacts of phytoplankton-derived organic matter on the properties of the primary marine aerosol–Part 2: Composition, hygroscopicity and cloud condensation activity, Atmos. Chem. Phys., 11, 2585-2602, https://doi.org/10.5194/acp-11-2585-2011, 2011.

Gao, W. H., Fan, J. W., Easter, R. C., Yang, Q., Zhao, C., and Ghan, S. J.: Coupling spectral-bin cloud microphysics with the MOSAIC aerosol model in WRF-Chem: Methodology and results for marine stratocumulus clouds, J. Adv. Model. Earth Syst., 8, 1289-1309, https://doi.org/10.1002/2016ms000676, 2016.

Grell, G. A. and Freitas, S. R.: A scale and aerosol aware stochastic convective parameterization for weather and air quality modeling, Atmos. Chem. Phys., 14, 5233–5250, https://doi.org/10.5194/acp-14-5233-2014, 2014.

Guenther, A., Karl, T., Harley, P., Wiedinmyer, C., Palmer, P. I., and Geron, C.: Estimates of global terrestrial isoprene emissions using MEGAN (Model of Emissions of Gases and Aerosols from Nature), Atmos. Chem. Phys., 6, 3181-3210, https://doi.org/10.5194/acp-6-3181-2006, 2006.

Haghighatnasab, M., Kretzschmar, J., Block, K., and Quaas, J.: Impact of Holuhraun volcano aerosols on clouds in cloud-system-resolving simulations, Atmos. Chem. Phys., 22, 8457-8472, https://doi.org/10.5194/acp-22-8457-2022, 2022.

Han, Q., Rossow, W. B., Chou, J., and Welch, R. M.: Global variation of column droplet concentration in low-level clouds, Geophys. Res. Lett., 25, 1419-1422, https://doi.org/10.1029/98GL01095, 1998.

Hu, Y. W., Zang, Z. L., Ma, X. Y., Li, Y., Liang, Y. F., You, W., Pan, X. B., and Li, Z. J.: Four-dimensional variational assimilation for SO2 emission and its application around the COVID-19 lockdown in the spring 2020 over China, Atmos. Chem. Phys., 22, 13183-13200, https://doi.org/10.5194/acp-22-13183-2022, 2022.

Hu, Z., Gao, S., Xue, F., and Yu, L.: Design and implementation of MICAPS4 web platform, J. Appl. Meteor. Sci., 29, 45, https://doi.org/10.11898/1001-7313.20180105, 2018.

Hudson, J. G. and Noble, S.: CCN and Vertical Velocity Influences on Droplet Concentrations and Supersaturations in Clean and Polluted Stratus Clouds, J. Atmos. Sci., 71, 312-331, https://doi.org/10.1175/JAS-D-13-086.1, 2014.

Huffman, G. J., Stocker, E. F., Bolvin, D. T., Nelkin, E. J., and Tan, J.: GPM IMERG Final Precipitation L3 1 day 0.1 degree x 0.1 degree V06, Edited by Andrey Savtchenko, Greenbelt, MD [dataset], https://doi.org/10.5067/GPM/IMERGDF/DAY/06, 2019.

Iacono, M. J., Delamere, J. S., Mlawer, E. J., Shephard, M. W., Clough, S. A., and Collins, W. D.: Radiative forcing by long-lived greenhouse gases: Calculations with the AER radiative transfer models, J. Geophys. Res.: Atmos., 113, D13103, https://doi.org/10.1029/2008JD009944, 2008.

IPCC: Climate Change 2023: Synthesis Report. Contribution of Working Groups I, II and III to the Sixth Assessment Report of the Intergovernmental Panel on Climate Change, IPCC, Geneva, Switzerland [report], 35-115, https://doi.org/10.59327/IPCC/AR6-9789291691647, 2023.

Jia, H., Ma, X., Yu, F., Liu, Y., and Yin, Y.: Distinct impacts of increased aerosols on cloud droplet number concentration of stratus/stratocumulus and cumulus, Geophys. Res. Lett., 46, 13517-13525, https://doi.org/10.1029/2019GL085081, 2019a.

Jia, H., Ma, X., and Liu, Y.: Exploring aerosol-cloud interaction using VOCALS-REx aircraft measurements, Atmos. Chem.

https://doi.org/10.5194/egusphere-2025-2555
Preprint. Discussion started: 15 July 2025


Phys., 19, 7955-7971, https://doi.org/10.5194/acp-19-7955-2019, 2019b.

Jia, H., Quaas, J., Gryspeerdt, E., Böhm, C., and Sourdeval, O.: Addressing the difficulties in quantifying droplet number response to aerosol from satellite observations, Atmos. Chem. Phys., 22, 7353-7372, https://doi.org/10.5194/acp-22-7353-2022, 2022.

Khain, A., Pokrovsky, A., Pinsky, M., Seifert, A., and Phillips, V.: Simulation of Effects of Atmospheric Aerosols on Deep Turbulent Convective Clouds Using a Spectral Microphysics Mixed-Phase Cumulus Cloud Model. Part I: Model Description and Possible Applications, J. Atmos. Sci., 61, 2963-2982, https://doi.org/10.1175/jas-3350.1, 2004.

Khain, A. P., Beheng, K. D., Heymsfield, A., Korolev, A., Krichak, S. O., Levin, Z., Pinsky, M., Phillips, V., Prabhakaran, T., Teller, A., van den Heever, S. C., and Yano, J. I.: Representation of microphysical processes in cloud-resolving models: Spectral (bin) microphysics versus bulk parameterization, Rev. Geophys., 53, 247-322, https://doi.org/10.1002/2014rg000468, 2015.

Levy, R., Hsu, C., Sayer, A., Mattoo, S., and Lee, J.: MODIS atmosphere L2 aerosol product. NASA MODIS adaptive processing system, Goddard Space Flight Center, USA [dataset], https://doi.org/10.5067/MODIS/MOD04_L2.061, 2015.

Li, M., Liu, H., Geng, G., Hong, C., Liu, F., Song, Y., Tong, D., Zheng, B., Cui, H., and Man, H.: Anthropogenic emission inventories in China: a review, Natl. Sci. Rev., 4, 834-866, https://doi.org/10.1093/nsr/nwx150, 2017.

Liu, Y., Lin, T., Zhang, J., Wang, F., Huang, Y., Wu, X., Ye, H., Zhang, G., Cao, X., and de Leeuw, G.: Opposite effects of aerosols and meteorological parameters on warm clouds in two contrasting regions over eastern China, Atmos. Chem. Phys., 24, 4651-4673, https://doi.org/10.5194/acp-24-4651-2024, 2024.

Lohmann, U. and Feichter, J.: Global indirect aerosol effects: a review, Atmos. Chem. Phys., 5, 715-737, https://doi.org/10.5194/acp-5-715-2005, 2005.

Ma, X., Jia, H., Yu, F., and Quaas, J.: Opposite aerosol index - cloud droplet effective radius correlations over major industrial regions and their adjacent oceans, Geophys. Res. Lett., 45, 5771-5778, https://doi.org/10.1029/2018GL077562, 2018.

McComiskey, A. and Feingold, G.: The scale problem in quantifying aerosol indirect effects, Atmos. Chem. Phys., 12, 1031-1049, https://doi.org/10.5194/acp-12-1031-2012, 2012.

Mlawer, E. J., Taubman, S. J., Brown, P. D., Iacono, M. J., and Clough, S. A.: Radiative transfer for inhomogeneous atmospheres: RRTM, a validated correlated-k model for the longwave, J. Geophys. Res.: Atmos., 102, 16663-16682, https://doi.org/https://doi.org/10.1029/97JD00237, 1997.

National Meteorological Centre of China: National Meteorological Centre official website, http://www.nmc.cn (last access: 19 March 2025), 2009.

NCEP/National Weather Service/NOAA/U.S. Department of Commerce: NCEP ADP Global Surface Observational Weather Data, NCAR [data set], https://doi.org/10.5065/4F4P-E398, 2004.

NCEP/National Weather Service/NOAA/U.S. Department of Commerce: NCEP GDAS/FNL 0.25 Degree Global Tropospheric Analyses and Forecast Grids, Research Data Archive at the National Center for Atmospheric Research, Computational and Information Systems Laboratory, NCAR [data set], https://doi.org/10.5065/D65Q4T4Z, 2015.

Niu, X., Ma, X., and Jia, H.: Analysis of cloud-type distribution characteristics over major aerosol emission regions in the Northern Hemisphere by using CloudSat/CALIPSO satellite data, J. Meteor. Sci., 42, 467-480, https://doi.org/10.12306/2021jms.0006, 2022.

Pahlow, M., Parlange, M. B., and Porté-Agel, F.: On Monin–Obukhov similarity in the stable atmospheric boundary layer, Boundary Layer Meteorol., 99, 225-248, https://doi.org/10.1023/A:1018909000098, 2001.

Pincus, R., Platnick, S., Ackerman, S. A., Hemler, R. S., and J., P. H. R.: Reconciling Simulated and Observed Views of Clouds: MODIS, ISCCP, and the Limits of Instrument Simulators, J. Clim., 25, 4699-4720,

https://doi.org/10.5194/egusphere-2025-2555
Preprint. Discussion started: 15 July 2025


https://doi.org/10.1175/JCLI-D-11-00267.1, 2012.

Platnick, S., Ackerman, S., King, M., Meyer, K., Menzel, W., Holz, R., Baum, B., and Yang, P.: MODIS atmosphere L2 cloud product (06_L2), NASA MODIS Adaptive Processing System, Goddard Space Flight Center, USA [data set], https://doi.org/10.5067/MODIS/MOD06_L2.061, 2015.

Quaas, J., Boucher, O., and Lohmann, U.: Constraining the total aerosol indirect effect in the LMDZ and ECHAM4 GCMs using MODIS satellite data, Atmos. Chem. Phys., 6, 947-955, https://doi.org/10.5194/acp-6-947-2006, 2006.

Reutter, P., Su, H., Trentmann, J., Simmel, M., Rose, D., Gunthe, S. S., Wernli, H., Andreae, M. O., and Pöschl, U.: Aerosol- and updraft-limited regimes of cloud droplet formation: influence of particle number, size and hygroscopicity on the activation of cloud condensation nuclei (CCN), Atmos. Chem. Phys., 9, 7067-7080, https://doi.org/10.5194/acp-9-7067-2009, 2009.

Roh, W., Satoh, M., Hashino, T., Okamoto, H., and Seiki, T.: Evaluations of the thermodynamic phases of clouds in a cloud-system-resolving model using CALIPSO and a satellite simulator over the Southern Ocean, J. Atmos. Sci., 77, 3781-3801, https://doi.org/10.1175/JAS-D-19-0273.1, 2020.

Sakaeda, N., Wood, R., and Rasch, P. J.: Direct and semidirect aerosol effects of southern African biomass burning aerosol, J. Geophys. Res.: Atmos., 116, https://doi.org/10.1029/2010JD015540, 2011.

Salma, I., Thén, W., Vörösmarty, M., and Gyöngyösi, A. Z.: Cloud activation properties of aerosol particles in a continental Central European urban environment, Atmos. Chem. Phys., 21, 11289-11302, https://doi.org/10.5194/acp-21-11289-2021, 2021.

Saponaro, G., Kolmonen, P., Sogacheva, L., Rodriguez, E., Virtanen, T., and de Leeuw, G.: Estimates of the aerosol indirect effect over the Baltic Sea region derived from 12 years of MODIS observations, Atmos. Chem. Phys., 17, 3133-3143, https://doi.org/10.5194/acp-17-3133-2017, 2017.

Satellite Services Division: Office of Satellite Data Processing and Distribution/NESDIS/NOAA/U.S. Department of Commerce, and National Centers for Environmental Prediction/National Weather Service/NOAA/U.S. Department of Commerce: NCEP ADP Global Upper Air Observational Weather Data, NCAR [data set], https://doi.org/10.5065/39C5-Z211, 2004.

Sha, T., Ma, X. Y., Jia, H. L., Tian, R., Chang, Y. H., Cao, F., and Zhang, Y. L.: Aerosol chemical component: Simulations with WRF-Chem and comparison with observations in Nanjing, Atmos. Environ., 218, 116982, https://doi.org/10.1016/j.atmosenv.2019.116982, 2019.

Sha, T., Ma, X. Y., Wang, J., Tian, R., Zhao, J. Q., Cao, F., and Zhang, Y. L.: Improvement of inorganic aerosol component in $PM_{2.5}$ by constraining aqueous-phase formation of sulfate in cloud with satellite retrievals: WRF-Chem simulations, Sci. Total Environ., 804, 150229, https://doi.org/10.1016/j.scitotenv.2021.150229, 2022.

Shin, H. H., Hong, S. Y., and Dudhia, J.: Impacts of the Lowest Model Level Height on the Performance of Planetary Boundary Layer Parameterizations, Mon. Weather Rev., 140, 664-682, https://doi.org/10.1175/mwr-d-11-00027.1, 2012.

Twomey, S.: The Influence of Pollution on the Shortwave Albedo of Clouds, J. Atmos. Sci., 34, 1149-1152, https://doi.org/10.1175/1520-0469(1977)034<1149:Tiopot>2.0.Co;2, 1977.

University Corporation for Atmospheric Research (UCAR): WRF Source Codes and Graphics Software Download Page [code], https://www2.mmm.ucar.edu/wrf/users/download/get_sources.html (last access: 22 June 2024), 2024.

Wild, O., Zhu, X., and Prather, M. J.: Fast-J: Accurate simulation of in-and below-cloud photolysis in tropospheric chemical models, J. Atmos. Chem., 37, 245-282, https://doi.org/10.1023/A:1006415919030, 2000.

Zaveri, R. A., Easter, R. C., Fast, J. D., and Peters, L. K.: Model for Simulating Aerosol Interactions and Chemistry (MOSAIC), J. Geophys. Res. D: Atmos., 113, D13204, https://doi.org/10.1029/2007jd008782, 2008.

https://doi.org/10.5194/egusphere-2025-2555
Preprint. Discussion started: 15 July 2025


Zelinka, M. D., Andrews, T., Forster, P. M., and Taylor, K. E.: Quantifying components of aerosol - cloud - radiation interactions in climate models, J. Geophys. Res.: Atmos., 119, 7599-7615, https://doi.org/10.1002/2014JD021710, 2014.

Zhang, Y. W., Fan, J. W., Li, Z. Q., and Rosenfeld, D.: Impacts of cloud microphysics parameterizations on simulated aerosol–cloud interactions for deep convective clouds over Houston, Atmos. Chem. Phys., 21, 2363-2381, https://doi.org/10.5194/acp-21-2363-2021, 2021.

Zhao, C., Liu, X., Leung, L. R., Johnson, B., McFarlane, S. A., Gustafson, W. I., Fast, J. D., and Easter, R.: The spatial distribution of mineral dust and its shortwave radiative forcing over North Africa: modeling sensitivities to dust emissions and aerosol size treatments, Atmos. Chem. Phys., 10, 8821-8838, https://doi.org/10.5194/acp-10-8821-2010, 2010.

Zhao, J., Ma, X., Wu, S., and Sha, T.: Dust emission and transport in Northwest China: WRF-Chem simulation and comparisons with multi-sensor observations, Atmos. Res., 241, 104978, https://doi.org/10.1016/j.atmosres.2020.104978, 2020.

Zhao, J., Ma, X., Quaas, J., and Jia, H.: Exploring aerosol–cloud interactions in liquid-phase clouds over eastern China and its adjacent ocean using the WRF-Chem–SBM model, Atmos. Chem. Phys., 24, 9101-9118, https://doi.org/10.5194/acp-24-9101-2024, 2024.

Zhao, J. Model output and namelist file for manuscript "Sensitivity of aerosol-cloud interactions to meteorological conditions in different environments", Zenodo [Data set], https://doi.org/10.5281/zenodo.15508465, 2025.

Zheng, B., Tong, D., Li, M., Liu, F., Hong, C., Geng, G., Li, H., Li, X., Peng, L., and Qi, J.: Trends in China's anthropogenic emissions since 2010 as the consequence of clean air actions, Atmos. Chem. Phys., 18, 14095-14111, https://doi.org/10.5194/acp-18-14095-2018, 2018.

Zheng, X., Xi, B., Dong, X., Wu, P., Logan, T., and Wang, Y.: Environmental effects on aerosol–cloud interaction in non-precipitating marine boundary layer (MBL) clouds over the eastern North Atlantic, Atmos. Chem. Phys., 22, 335-354, https://doi.org/10.5194/acp-22-335-2022, 2022.

Zhong, X. h., Ruiz-Arias, J. A., and Kleissl, J.: Dissecting surface clear sky irradiance bias in numerical weather prediction: Application and corrections to the New Goddard Shortwave Scheme, Sol. Energy, 132, 103-113, https://doi.org/10.1016/j.solener.2016.03.009, 2016.